

A dynamic zone defines interneuron remodeling in the adult neocortex

Wei-Chung Allen Lee^{a,b}, Jerry L. Chen^{a,c}, Hayden Huang^{d,1}, Jennifer H. Leslie^{a,c}, Yael Amitai^{b,e}, Peter T. So^d, and Elly Nedivi^{a,b,c,2}

^aThe Picower Institute for Learning and Memory and Departments of ^bBrain and Cognitive Sciences, ^cBiology, and ^dMechanical Engineering, Massachusetts Institute of Technology, Cambridge, MA 02139; and ^eDepartment of Physiology, Faculty of Health Sciences, Ben-Gurion University, Beer-Sheva 84105, Israel

Communicated by Robert Desimone, Massachusetts Institute of Technology, Cambridge, MA, October 13, 2008 (received for review February 20, 2008)

The contribution of structural remodeling to long-term adult brain plasticity is unclear. Here, we investigate features of GABAergic interneuron dendrite dynamics and extract clues regarding its potential role in cortical function and circuit plasticity. We show that remodeling interneurons are contained within a “dynamic zone” corresponding to a superficial strip of layers 2/3, and remodeling dendrites respect the lower border of this zone. Remodeling occurs primarily at the periphery of dendritic fields with addition and retraction of new branch tips. We further show that dendrite remodeling is not intrinsic to a specific interneuron class. These data suggest that interneuron remodeling is not a feature predetermined by genetic lineage, but rather, it is imposed by cortical laminar circuitry. Our findings are consistent with dynamic GABAergic modulation of feedforward and recurrent connections in response to top-down feedback and suggest a structural component to functional plasticity of supragranular neocortical laminae.

dendrite | inhibitory | plasticity | two-photon microscopy | visual cortex

Despite decades of evidence for functional plasticity of the adult brain, manifested in our ability to learn and the continual adaptation of primary sensory maps (1, 2), the existence and role of structural remodeling (3, 4) in circuit plasticity remains controversial. Structural plasticity of excitatory projection neurons that enables circuit remodeling during development wanes as “critical periods” close and circuits mature, suggesting that in the adult, other mechanisms are likely recruited for functional remodeling.

To investigate the extent of structural plasticity in the mammalian brain, we previously used a multiphoton microscope system for chronic *in vivo* imaging of neuronal morphology in the intact rodent cerebral cortex (5). Using this system, we imaged and reconstructed the dendritic trees of neurons in visual cortex of *thy1*-GFP-S transgenic mice (6). These mice express GFP in a random subset of neurons sparsely distributed within the superficial cortical layers that are optically accessible through surgically implanted cranial windows. This enables examination of dendritic branch dynamics in individual neurons over several months. Our results confirmed recent *in vivo* imaging studies showing that excitatory projection neurons show little, if any, change in branch tip length over time (7, 8). Surprisingly, we found that GABAergic interneurons in layer (L) 2/3 of visual cortex undergo arbor remodeling occurring over days to weeks (5). Although most work related to circuit plasticity in the adult brain has focused on excitatory connectivity, inhibition is clearly critical for mature circuit function. The superficial neocortical layers contain a remarkably heterogeneous population of nonpyramidal interneurons that differ in their cellular targeting and hence function within the cortical circuit (9–11) and may not be uniform in their propensity for structural change. Stratification of the mammalian neocortex into cytoarchitectonic and functionally distinct layers raises the possibility that interneuron structural plasticity may also be regulated by laminar position or functional domain.

We obtained the surprising result that interneuron remodeling is most pronounced in a ‘dynamic zone’ that corresponds to superficial L2/3, and is not restricted to specific interneuron subtypes. This suggests that although structural plasticity in the adult is specific to

interneurons, it is not a function of physiological or genetic subtype, but is regulated by neocortical circuit architecture.

Results

Dynamics as a Function of Laminar Position. To test whether dendritic structural remodeling is cell type-specific and/or influenced by laminar location, we monitored over time the dendritic arbors of nonpyramidal neurons of heterogeneous morphology at various depths from the pial surface (see Fig. S1, Movie S1, Movie S2, Movie S3, and Movie S4).

Comparing interneuron dendrite dynamics at different depths from the pial surface, we observed that shallow ($< 60 \mu\text{m}$) and deep ($> 150 \mu\text{m}$) interneurons were more stable than interneurons with somata between 60 – $150 \mu\text{m}$ from the pial surface (Fig. 1A). We quantified the structural dynamics of each cell by calculating the Fano Factor (FF), which compares the change or variance relative to the mean (12) for each monitored dendrite branch tip, averaged across all of the dendrites of a given cell. A FF above 0.35 corresponded to cells with dynamic branches (see SI Methods, Fig. S2, and Table S1). Shallow and deep interneurons had low FFs, indicating a high degree of arbor stability (shallow: $n = 85$ dendrites on 7 cells, mean FF = 0.15, SEM = 0.036; deep: $n = 141$ dendrites on 9 cells, mean FF = 0.28, SEM = 0.054), similar to that of pyramidal cells ($n = 182$ dendrites on 10 cells, mean FF = 0.21, SEM = 0.018, $P > 0.3$, ANOVA). In contrast, interneurons whose cell bodies resided in a band between 60 – $150 \mu\text{m}$ from the pial surface (corresponding to superficial L2/3) had dynamic branch tips with FFs that were significantly higher than pyramidal cells and interneurons in L1 or deep L2/3 ($n = 327$ dendrites on 16 cells, mean FF = 0.68, SEM = 0.059; $*, P < 0.0001$, ANOVA and Fisher post-hoc test) (Fig. 1B). These data indicate that laminar position may regulate interneuron structural plasticity.

Dynamics Is Greatest for Short, Distal Branch Tips. Comparing multiple dendrite parameters, we identified features that differentiate dynamic from stable branches on the same remodeling interneurons. Cumulative probability distributions of mean and minimum dynamic branch tip lengths were both significantly different from those of stable branch tips and clearly skewed toward shorter lengths, indicating that dynamic tips tend to be shorter than stable tips. Approximately 40% of dynamic branch tips had a minimum length of zero, indicating branch tip additions and/or eliminations (Fig. 2A and B). The cumulative probability distributions of branch tip distance to the somatic center of mass show that dynamic

Author contributions: W.-C.A.L. and E.N. designed research; W.-C.A.L., J.L.C., and J.H.L. performed research; H.H. and P.T.S. contributed new reagents/analytic tools; W.-C.A.L., J.L.C., J.H.L., and Y.A. analyzed data; and W.-C.A.L. and E.N. wrote the paper.

The authors declare no conflict of interest.

¹Present address: Brigham and Women’s Hospital, Cambridge, MA 02139.

²To whom correspondence should be addressed at: Massachusetts Institute of Technology, 46-3239, 43 Vassar Street, Cambridge, MA 02139. E-mail: nedivi@mit.edu.

This article contains supporting information online at www.pnas.org/cgi/content/full/0810149105/DCSupplemental.

© 2008 by The National Academy of Sciences of the USA

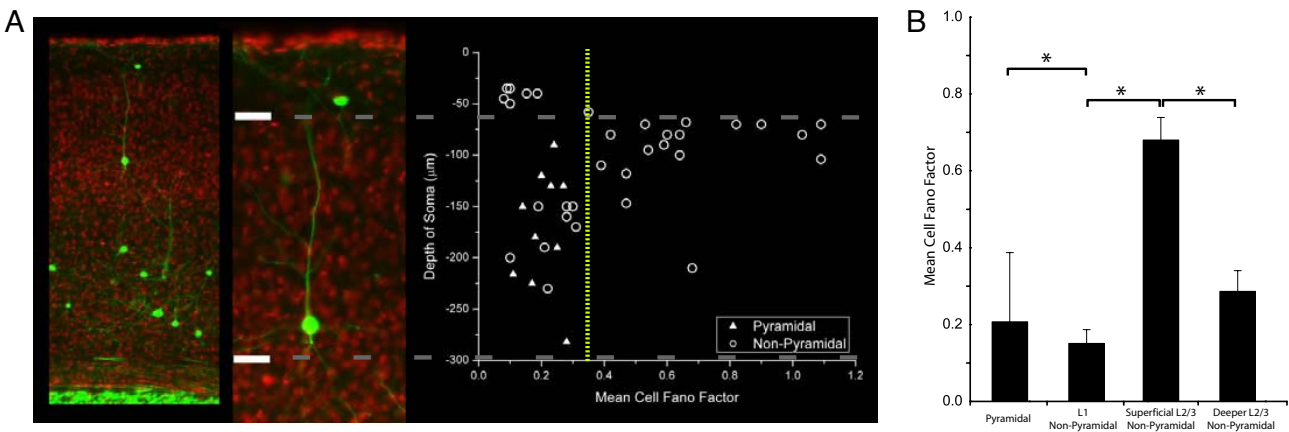


Fig. 1. Laminar specificity of nonpyramidal dendritic arbor remodeling. (A) Low- and high-magnification of an epi-fluorescence photomicrograph from a coronal section containing the chronically imaged nonpyramidal cell “stdy” visualized by GFP expression (in green) and overlaid with DAPI (in red) staining allowing discrimination of neocortical lamina. To the right the mean FF is plotted for all of the monitored branch tips belonging to each cell as a function of the depth of its cell soma. The yellow dotted line corresponds to a mean cell FF of 0.35, which separates stable ($FF \leq 0.35$) from dynamic ($FF > 0.35$) cells. (B) Quantification of mean FF between shallow L1 ($<60 \mu\text{m}$ from the pial surface), superficial L2/3 ($>60 \mu\text{m}$ and $<150 \mu\text{m}$), and deep L2/3 ($>150 \mu\text{m}$) nonpyramidal cells ($n = 42$ cells, $*$, $P < 0.0001$, ANOVA and Fisher post-hoc test).

branches are located further from the cell body than are stable branch tips (Fig. 2C). Other branch tip parameters, such as branch order, tortuosity, and location within the x -, y -, or z -dimensions, were not significantly different between stable and dynamic branches ($P > 0.2$, Kolmogorov-Smirnov test). This suggests dynamic branch tips tend to occur at the periphery of the dendritic field.

Dynamic Branch Tips Respect the Dynamic Zone Deep Border. With distal branch tips appearing most dynamic, we examined whether these branch tip parameters, such as branch order, tortuosity, and location within the x -, y -, or z -dimensions, were not significantly different between stable and dynamic branches ($P > 0.2$, Kolmogorov-Smirnov test). This suggests dynamic branch tips tend to occur at the periphery of the dendritic field.

Interneuron Dynamics Are Not Restricted to a Morphological Subtype. To examine whether dendritic remodeling is specific to interneuron subtype, we used principal component analysis (PCA) and cluster analysis on morphometric data from chronically imaged neurons of *thy1-GFP-S* mice *in vivo* and from neurons in fixed brains of “GIN” mice (13) imaged once *ex vivo*. In GIN mice, GFP is expressed in somatostatin-positive interneurons defined morphologically as Martinotti cells (14). The Martinotti cells from the GIN mice served as a relatively homogeneous control group to test the validity of the cluster analysis and were used only for this analysis.

The dendrogram in Fig. 3 shows the relative linkage distance

between 42 chronically imaged neurons and 3 reconstructed neurons from GIN mice following unsupervised cluster analysis. There is a clear and early distinction between pyramidal (black branch) and nonpyramidal cells (green, blue, and red branches). The far-right branch represents 10 pyramidal cells and one nonpyramidal cell whose bipolar dendritic profile clustered with pyramidal cells. The left branch corresponds to the 31 chronically imaged interneurons and 3 putative Martinotti cells. The chronically imaged interneurons appear to cluster in at least 3 categories. The right branch (red) contains nonpyramidal cells with generally small-to medium-sized dendritic fields of moderate tortuosity and moderate- to high-branch density. The left cluster (green) is identified by arbors of small to moderate size with tortuous and dense branching patterns. The middle branch (blue) includes interneurons with larger, sparse dendritic fields with longer more linear dendritic segments. This cluster contained the Martinotti cells. Their co-clustering confirms the usefulness of our cluster analysis as a classification scheme. The three interneuron classes represented by the green, red, and blue branches of the dendrogram each contain dynamic as well as nondynamic cells, dependent on depth (see FF and depth labeling for individual cells, Fig. 3). It is apparent that within this scheme dynamic cells populate all interneuron classes, suggesting that dendritic arbor dynamics is not regulated by interneuron subtype.

Multiple Interneuron Immunohistochemical Subtypes in the Dynamic Zone. Because dendritic morphology alone is not considered a definitive indicator of interneuron subtype, it is possible that

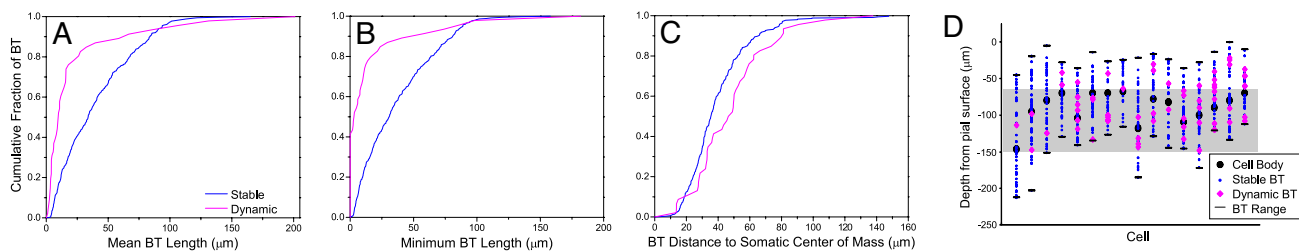


Fig. 2. Morphometric features of dynamic branch tips. The cumulative fraction of the total number of stable and dynamic branch tips from dynamic cells is plotted for mean (A) and minimum (B) BTLs, and distance from the center of mass of the soma (C). Stable and dynamic branch tip distributions are significantly different for each measure ($n = 327$ branch tips; Mean and Minimum BTL: $P < 0.0001$; Distance from Soma: $P < 0.01$; Kolmogorov-Smirnov test). (D) The depth of the distal terminus for each monitored branch tip for all dynamic interneurons is plotted showing stable (blue dots) and dynamic tips (magenta diamonds). Black spheres represent cell bodies. Gray shading represents the “dynamic zone”.

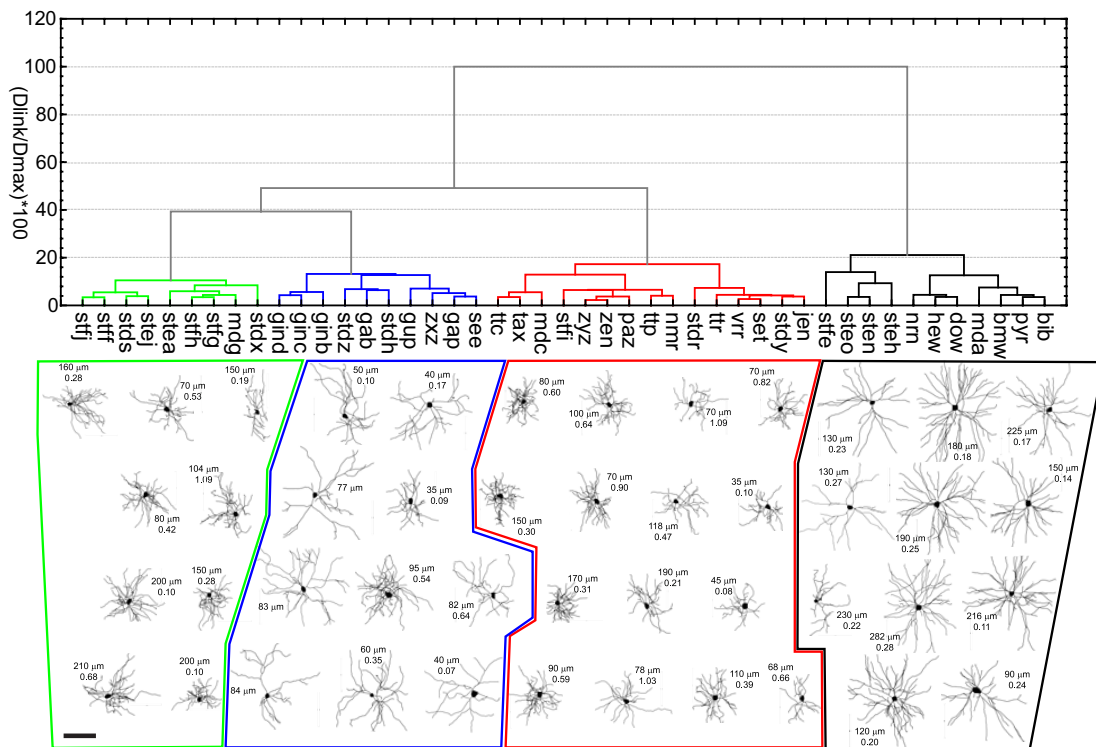


Fig. 3. Morphological cluster analysis of imaged cells. On the top is a cluster analysis dendrogram representing 11 morphometric variables selected after principal component analysis on 46 original somatic and dendritic variables. These 11 variable accounted for 89% of the total variance. Representative reconstructions from 42 time-lapse imaged neurons and three putative Martinotti cells from "GIN" mice ("ginb", "ginc", and "gind" not time-lapse imaged) clustered, each individually named with a 3–4 character delimiter. Below are dorsal views of representative 2-D projections of the 3-D traces of these neurons in their order of appearance in the tree. Each chronically imaged neuron is labeled with its depth from the pial surface and mean cell FF across its monitored branch tips. (Scale bar, 100 μ m.)

GFP-expressing nonpyramidal cells in the dynamic zone are disproportionately represented by specific interneuron subtypes based on other criteria. To address this possibility we performed immunohistochemistry on brain sections with an array of antibodies against interneuron markers. We found that the distribution of calretinin, and VIP expression in the GABAergic cell population was relatively uniform across L1, superficial L2/3 (top 100 μ m), and deep L2/3 (Fig. 4A). Somatostatin was twice as dense throughout

L2/3 compared with L1. Parvalbumin was the most unevenly distributed marker across these areas, colocalizing with approximately 40% of GABAergic neurons in deeper L2/3, approximately 24% in superficial L2/3, and approximately 3% L1. Examining the distribution of parvalbumin-, somatostatin-, calretinin-, and VIP-stained cells within the GFP-labeled population compared with the general GABAergic population in superficial L2/3 revealed no significant differences in subtype representation (Fig. 4B, parvalbumin $n = 9$ animals, $P = 0.92$; somatostatin $n = 9$ animals, $P = 0.89$; calretinin $n = 9$ animals, $P = 0.56$; VIP $n = 12$ animals, $P = 0.79$; two-tailed Student's t test). Our data shows that dendritic remodeling spans multiple immunohistochemical and morphological subtypes.

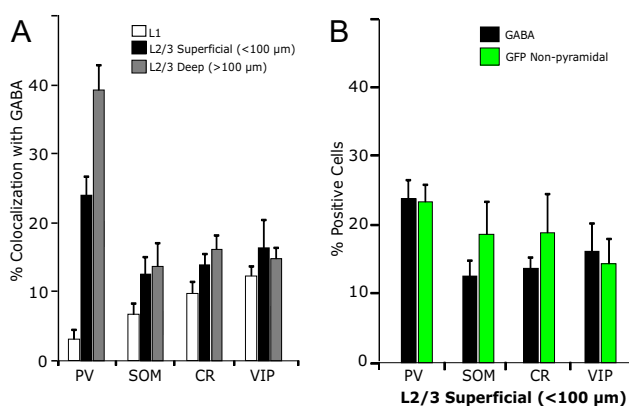
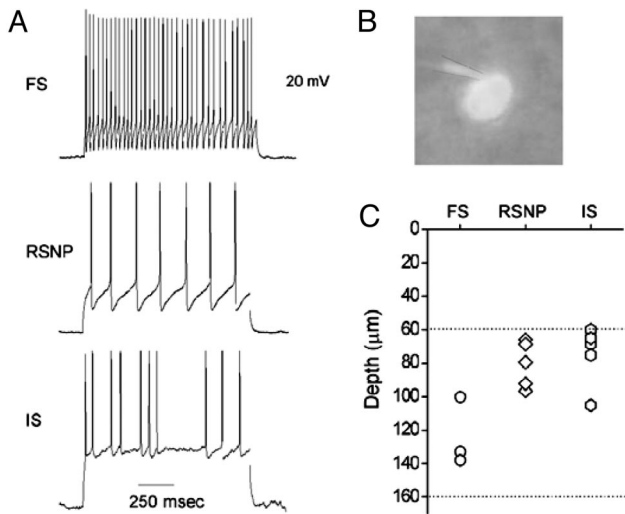


Fig. 4. Distribution of interneuron subtype markers in the superficial layers of mouse visual cortex. (A) Plot showing the distribution of GABA-positive cells colabeling for parvalbumin (PV), somatostatin (SOM), calretinin (CR), and vasointestinal peptide (VIP) in L1, superficial L2/3 and deep L2/3 of mouse visual cortex ($n = 2758$ immunopositive cells from six animals). (B) The representation of interneuron subtypes within the GFP nonpyramidal cell population in superficial L2/3 compared with their representation in the general GABAergic cell population ($n = 1066$ GFP nonpyramidal cells from 12 animals).

Multiple Physiological Interneuron Subtypes in the Dynamic Zone. Subtypes of cortical interneurons can also be grouped by their characteristic firing patterns (15, 16). We recorded from GFP-expressing interneurons in the dynamic zone in acute slices of visual cortex. Depolarizing neurons by current steps revealed variable firing patterns. For the purpose of this study we divided these patterns into three subtypes (Fig. 5 A and B): (i) Fast spiking (FS) neurons exhibited narrow (< 2 ms at the base) action potentials followed by prominent after-hyperpolarizations (AHPs) and could sustain nonaccommodating high frequency firing (16–18). This firing pattern is most commonly associated with parvalbumin-expressing cells (16, 19). (ii) Regular spiking nonpyramidal (RSNP) neurons had broader spikes followed by prominent AHPs, their spike trains displayed various degrees of accommodation, and their firing frequency did not exceed a few tens of Hertz (16, 17). Similar firing behavior has been described in somatostatin- or calretinin-expressing neurons (14, 16). (iii) Irregular spiking (IS) neurons did not fall into either of these two categories, and most noticeably these neurons exhibited irregular spike trains, compatible with firing

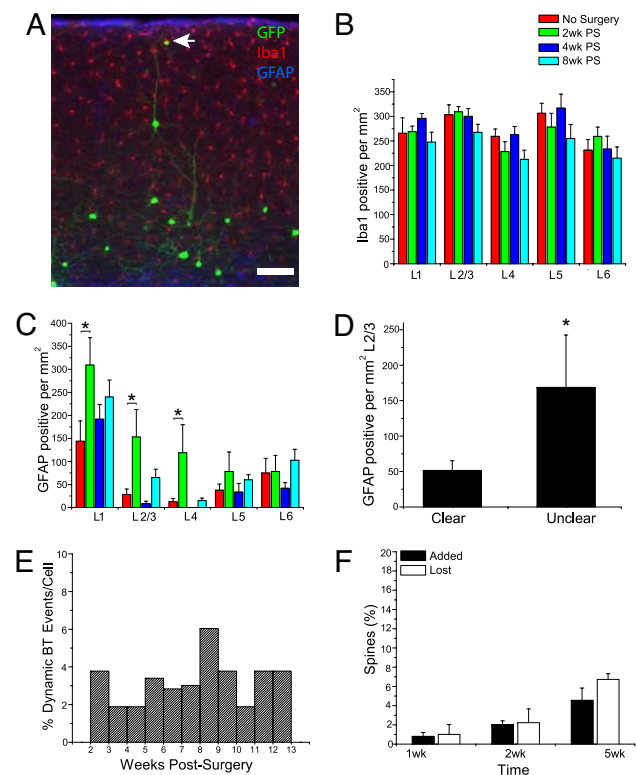


patterns of VIP or calretinin containing neurons (16, 20). Overall, our recordings imply that GFP-expressing interneurons in the dynamic zone of the *thy1*-GFP-S mouse represent a highly heterogeneous population, including most described interneuron subtypes (Fig. 5C).

Effects of Cranial Window Insertion on *In Vivo* Imaging of Neuronal Structure. Recently, it was reported that time-lapse *in vivo* imaging using cranial windows may transiently enhance dendritic spine dynamics correlated with activation of an immune response (21). Given the importance of this preparation for our studies, we sought to address potential problems associated with the use of cranial windows. We performed immunohistochemistry using antibodies against ionizing calcium-binding adaptor molecule 1 (Iba1) to visualize microglia (22) and glial fibrillary acidic protein (GFAP) to label astrocytes (23) in brain sections from chronically imaged animals [8-weeks post-surgery (PS) $n = 1$; 11 weeks PS, $n = 2$]. None of the chronically imaged brains showed enhanced astrocyte or microglial activation in the region below the cranial window around the imaged cells (Fig. 6 and Fig. S3).

Because cranial windows can be opaque immediately after surgery, we wait at least 2 weeks, but more typically 3–4 weeks post-surgery (PS) to allow window clearing before imaging. To determine whether window clearing may be related to the cessation of an immune response, we performed immunohistochemistry on brains 2, 4, and 8 weeks PS and on control brains from animals without window surgery (Fig. S3). Microglia staining at any time point PS did not differ from controls (Fig. 6A and B and Fig. S3). Astrocyte immunoreactivity increased significantly in L1–L4 when compared with controls at 2 weeks, but not at 4 or 8 weeks PS (Fig. 6A and C and Fig. S3). Numbers of GFAP immunopositive cells were significantly higher underneath unclear as compared with clear windows (Fig. 6D and Fig. S3), such that window clarity was a negative indicator of astrocyte activation. These results demonstrate that any immune response elicited by cranial window surgery largely subsides by 2 weeks PS, and is undetectable in animals with optically clear windows at 3–4 weeks PS (see *SI Methods* for details).

If the immune response affects dendrite dynamics one would



expect to observe more dynamic events closer to the time of surgery (21). We compared both interneuron dendritic arbor and pyramidal neuron dendritic spine dynamics as a function of time after surgery, and found that changes occur fairly uniformly in the weeks to months after surgery (Fig. 6E). Rates of spine addition and elimination on L2/3 pyramidal cells were low (98% stable spines at 1 week, 96% at 2 weeks, and 89% at 5 weeks) (Fig. 6F), consistent with imaging data from the adult visual cortex using both thin-skull and cranial window preparations (21, 24–27). These data suggest that cranial window insertion by our protocol does not affect dendritic arbor or spine dynamics directly or through recruitment of an immune response.

Discussion

Here, we examine nonpyramidal cell dendritic arbor remodeling in the adult visual cortex to elucidate its possible function. We find that interneurons most often remodel short branches at the periphery of their dendritic fields with a relative balance of elonga-

tions and retractions, and that the FF is a useful quantitative measure for such dynamic branch tips. Stable and dynamic interneurons stratify by neocortical lamina, with remodeling interneurons localized to a dynamic zone corresponding to upper L2/3, starting at the interface with L1 and extending approximately 100 microns in depth. Cluster analysis, immunohistochemistry, and electrophysiology all show that interneuron remodeling is not restricted by subclass. Finally, we confirm that cranial windows do not cause measurable induction of inflammatory markers and are unlikely to generate artifactual plasticity during our *in vivo* time-lapse imaging (this issue is further discussed in *SI Methods*).

Dynamic Interneurons Are Not Subclass Specific. A central theme in cortical processing is the relationship between cell type and function. Considerable effort has been devoted to characterizing and delineating interneuron subtypes with the underlying hypothesis that each subtype plays a different role in cortical processing. Although some have argued that interneurons represent a continuum of diversity (28), anatomists, physiologists, and developmental biologists have proposed classifications based on morphology, physiological parameters, developmental origin, and gene expression (9–11). Today, it is clear that many of these attributes exhibit considerable overlap. Although our previous studies showed that the nonpyramidal GFP cells imaged *in vivo* are GABAergic (5) it is currently not feasible to examine all subtype markers in a single imaged neuron. We therefore studied in detail the GFP nonpyramidal population in superficial L2/3 of the *thy1-GFP-S* mice. Comparing GABAergic and GFP nonpyramidal neurons we found that representation of parvalbumin, somatostatin, calretinin, and VIP within the GFP population was statistically indistinguishable from their representation in the general GABAergic population. Recording from GFP-labeled cells in superficial L2/3 also shows representation of multiple firing pattern subtypes. Thus, the interneurons sampled in the imaged GFP population within the dynamic zone likely represent a broad spectrum of properties compatible with many previously described subclasses.

The PCA and cluster analysis of the imaged neurons based on their dendritic morphology is consistent with the immunocytochemical and electrophysiological data. Axonal morphology has been the morphological parameter best shown to correlate with interneuron subtypes classified by firing patterns and molecular markers (29). Classification by dendritic morphology alone has been argued to be an imperfect indicator of established interneuron subtypes (30, 31). Nonetheless, it was recently shown that the initial branching pattern, internode interval and spine density can be used to divide nonpyramidal cells into three dendritic types, correlated with axonal, neurochemical, and firing types (32). We found that an unsupervised cluster analysis of imaged neurons can distinguish between pyramidal cells and nonpyramidal cells, with the nonpyramidal cell group further segregating into three well-defined clusters. Although it has yet to be determined whether the nonpyramidal cell clusters each correspond to conventional interneuron subclasses, the fact that the Martinotti cells coclustered within one group suggests that they may. Because remodeling interneurons can be found within multiple subgroups, it seems likely that dendritic remodeling is not restricted to a particular interneuron subclass. Although interneuron subtypes may have diverse functions in the network based on physiology and axon connectivity, their dendritic fields appear similarly flexible.

Laminar Specificity of Interneuron Structural Plasticity. The neocortex is organized into distinct lamina with varying anatomical, functional, and developmental properties. Here, we show that nonpyramidal cells residing in a “dynamic zone” corresponding to superficial L2/3 are structurally dynamic whereas those above and below them are not. Dendrites of dynamic zone interneurons that extend into deep L2/3 are stable, but those within L2/3 and extending into L1 are free to remodel. Lower L1, immediately

adjacent to the dynamic zone, receives projections from L5 and is generally known as a locus for feedback connections from higher order brain areas important for top-down information like attention and context (33, 34). Tracing experiments in rodent visual cortex (35) indicate that feedforward connectivity into the dynamic zone in upper L2/3 comes mainly from lower L2/3. Upper L2/3 also has significant recurrent connectivity within the layer. Although it is argued that thalamic input reaches neurons in all of the neocortical lamina, the dynamic zone has perhaps the sparsest innervation by thalamo-cortical afferents (36, 37). This zone appears to be one of the few cortical regions to simultaneously process horizontal information (from L2/3) and feedback information from both the primary cortical output layer (L5) and higher cortical areas, all with little direct influence from the thalamus.

Electrophysiological studies have identified the intrinsic horizontal projections in L2/3 as the potential site for reorganization of sensory and motor maps in the adult neocortex (38–41). Although axon remodeling has been demonstrated in this locale (3, 4, 42, 43), lack of evidence for changes in the dendritic structure of pyramidal neurons gave rise to the idea that map plasticity derives from unmasking of latent horizontal pathways (44, 45) and is regulated by local inhibitory circuit neurons. Small adjustments in inhibitory tone could be sufficient to reweigh local connections and recalibrate cortical maps. Our finding of interneuron dendritic remodeling specifically in the cortical lamina where inhibition plays a critical role in adjusting map representations suggests that whereas first-order thalamo-cortical afferents may act as a stable infrastructure for cortical introduction of bottom-up information, dynamic zone interneurons and their dendrites in L1 and superficial L2/3 may be key players in recalibrating functional maps over time, through repeated normalization of existing templates to new input.

Given the sparse connectivity of the mammalian cerebral cortex, the capacity to physically modify cortical circuits even on a small, local scale could provide a substantial boost in information storage capacity, but would likely require repeated generate-and-test opportunities to select appropriate new synaptic partners (46). Within the dynamic zone we found every interneuron remodeling at least one dendrite (average of 4 remodeling dendrites per cell). The average change in nonpyramidal dendrite length was approximately 15 $\mu\text{m}/\text{dendrite}$ (range between 4 and 92 μm). Because synapse densities on nonpyramidal dendrites are estimated at approximately one synapse per μm (Kubota Y, personal communication) and interneurons constitute approximately 25% of cortical neurons (47), we can extrapolate that at least 60 synapses may be remodeling on every fourth or fifth cell at any given time. The question remains whether synaptic changes on this scale are sufficient to modulate inhibitory tone to an extent that would gradually recalibrate local map representations. It is useful to remember that the remodeling we report here is *not* in response to peripheral intervention and the potential for more extensive remodeling could become evident with visual perturbations that give rise to large-scale functional plasticity.

Materials and Methods

Animal Surgery and Two-Photon Imaging. To allow long-term visualization of *in vivo* neuronal morphology cranial windows were bilaterally implanted over the visual cortices of adult *thy1-GFP-S* mice (6) as previously described (5). Two to four weeks later, optically clear windows were selected for *in vivo* two-photon imaging, performed by using a custom-built microscope and acquisition software (5). Sulfamethoxazole (1 mg/ml) and trimethoprim (0.2 mg/ml) were chronically administered in the drinking water of mice with cranial windows through the final imaging session. Additional detail is provided in *SI Methods*.

Image Acquisition and Analysis. Raw scanner data were processed in Matlab (Mathworks) and ImageJ (National Institutes of Health). Individual image planes were stitched together to produce a 3×3 montage of adjoining x-y sections at a given depth from the pial surface. Four-dimensional (x, y, z , and t) stacks were traced and analyzed blind to age by using Object-Image (<http://simon.bio.uva.nl/object-image.html>) (48) and Neurolucida (MicroBrightField, Inc). For a sample of

z stacks and rotating 3-D reconstructions comparing an interneuron in superficial L2/3 with one in deep L2/3, see *Movie S1*, *Movie S2*, *Movie S3*, and *Movie S4*.

Dendritic branch analysis (pyramidal and nonpyramidal cells) included data from 384 monitored branch tips from 14 previously published cells in 13 animals (5) with an additional 610 branch tips from 28 cells in 25 animals ranging in age from 7–23 weeks postnatal (*SI Methods* and *Table S1*). The FF was computed for each individual branch tip, and then averaged for each cell across all its monitored dendrites to determine the mean cellular FF. The FF is defined as the variance in length of an individual branch tip, divided by the mean length of that branch tip [$FF = S^2/\bar{X}$, where $S^2 = \sum(X - \bar{X})^2/(n - 1)$]. See *SI Methods* for more detail.

Analysis of spine turnover was as described previously (7, 24–27). All monitored spines were on L2/3 pyramidal cells and were identified and tracked manually by using Object-Image.

Immunohistochemistry. Immunohistochemistry was performed on transcardially perfused and fixed brains essentially as described (5). For list of antibodies, see *SI Methods*. Chronically imaged cells were identified by location, morphology, and local landmarks. Images were collected on an upright epi-fluorescence scope (Nikon) using a $10\times$ /N.A. 0.3 (Nikon); $20\times$ /N.A. 0.75 (Nikon); or $40\times$ /N.A. 1.30 (Nikon) objective.

Principal Component and Cluster Analysis. Because of low GFP signal in 'GIN' mice (13) (Jackson Laboratory, backcross-ed to a C57BL/6 background), we imaged the morphology of GFP expressing Martinotti cells *in situ* in perfused brains through a cranial window similarly to our chronic imaging *in vivo*. GIN mice structural data were used exclusively for the cluster analysis in Fig. 3.

Forty-six morphological parameters were determined from 3-D reconstructions and used for PCA and cluster analysis essentially as previously described (29, 49) (see *SI Methods*). Morphometric data were transformed into standard scores by using the standard formula $(x_i - \bar{x})/S$ in an attempt to eliminate

arbitrary effects of units and to weigh variables equally. PCA and cluster analysis were performed with the Statistica software package (Statsoft, Inc.) (see *SI Methods*). After PCA, 11 of the original 46 variables accounting for 89% of the variance were selected for cluster analysis by using Ward's method (50) (to minimize the variance within each cluster) and Euclidean distances.

Recording from GFP-Labeled Cells in Slices. Standard methods were used to cut 300- μ m thick coronal slices of visual cortex from male *thy1-GFP-S* mice (14–21 days old). Whole cell recordings were performed with patch pipettes (5–7 M Ω), containing (in mM): 130 K-gluconate, 4 KCl, 2 NaCl, 10 Hepes, 0.2 EGTA, 4 ATP-Mg, 0.3 GTP-Tris, 7 phosphocreatine-Tris, 10 sucrose, and 0.25–0.5% Neurobiotin (Vector Labs), pH 7.25, 270 mOsm. GFP-expressing interneurons in L2/3 adjacent to the border with L1 were identified under fluorescence and then patched under IR/DIC optics by using a black and white CCD camera (CCD-300IFG, Dage-MTI). Voltage traces were recorded by using a patch-clamp amplifier (AxoPatch 2B, Axon Instruments) and analyzed off-line by using LabView-based software. After recording, brain slices were fixed and processed for neurobiotin by using standard procedures to reveal cellular morphology and location. Background staining with DAPI revealed cortical layers. Cell depth was normalized to the *in vivo* data by calculating a ratio of L1 measured in the fixed slice/60 μ m, the average width of L1 measured by two-photon *in vivo* imaging.

ACKNOWLEDGMENTS. We thank J. Gibson, T. Fujino, W. Lin, and E. Miller for comments on the manuscript; E. N. Brown for thoughtful suggestions regarding statistics and critical reading of the manuscript; J. Cha for multiphoton microscopy support; C. Jackson and I. Hutchings for excellent technical immunohistochemistry assistance; and Dean Bob Silbey for his enabling support of the *in vivo* imaging project. This work was sponsored by grants R03 EY014891 and R01 EY017656 from the National Eye Institute (to E.N.). H.H. was supported in part by National Institute for Biomedical Imaging and Bioengineering Grant R21 EB004646.

1. Bliss TV, Collingridge GL (1993) A synaptic model of memory: Long-term potentiation in the hippocampus. *Nature* 361:31–39.
2. Buonomano DV, Merzenich MM (1998) Cortical plasticity: From synapses to maps. *Annu Rev Neurosci* 21:149–186.
3. Florence SL, Taub HB, Kaas JH (1998) Large-scale sprouting of cortical connections after peripheral injury in adult macaque monkeys. *Science* 282:1117–1120.
4. Darian-Smith C, Gilbert CD (1994) Axonal sprouting accompanies functional reorganization in adult cat striate cortex. *Nature* 368:737–740.
5. Lee WC, et al. (2006) Dynamical remodeling of dendritic arbors in GABAergic interneurons of adult visual cortex. *PLoS Biol* 4:e29.
6. Feng G, et al. (2000) Imaging neuronal subsets in transgenic mice expressing multiple spectral variants of GFP. *Neuron* 28:41–45.
7. Trachtenberg JT, et al. (2002) Long-term *in vivo* imaging of experience-dependent synaptic plasticity in adult cortex. *Nature* 420:788–794.
8. Mizrahi A, Katz LC (2003) Dendritic stability in the adult olfactory bulb. *Nat Neurosci* 6:1201–1207.
9. Kawaguchi Y, Kondo S (2002) Parvalbumin, somatostatin, and cholecystokinin as chemical markers for specific GABAergic interneuron types in the rat frontal cortex. *J Neurocytol* 31:277–287.
10. Markram H, et al. (2004) Interneurons of the neocortical inhibitory system. *Nat Rev Neurosci* 5:793–807.
11. Huang ZJ, Di Cristo G, Ango F (2007) Development of GABA innervation in the cerebral and cerebellar cortices. *Nat Rev Neurosci* 8:673–686.
12. Teich MC, Turcott RG, Siegel RM (1996) Temporal correlation in cat striate-cortex neural spike trains. *IEEE Eng Med Biol* 15:79–87.
13. Oliva AA Jr, Jiang M, Lam T, Smith KL, Swann JW (2000) Novel hippocampal interneuronal subtypes identified using transgenic mice that express green fluorescent protein in GABAergic interneurons. *J Neurosci* 20:3354–3368.
14. Xu X, Roby KD, Callaway EM (2006) Mouse cortical inhibitory neuron type that coexpresses somatostatin and calretinin. *J Comp Neurol* 499:144–160.
15. Kawaguchi Y (1993) Physiological, morphological, and histochemical characterization of three classes of interneurons in rat neostriatum. *J Neurosci* 13:4908–4923.
16. Cauli B, et al. (1997) Molecular and physiological diversity of cortical nonpyramidal cells. *J Neurosci* 17:3894–3906.
17. Kawaguchi Y (1995) Physiological subgroups of nonpyramidal cells with specific morphological characteristics in layer I/II of rat frontal cortex. *J Neurosci* 15:2638–2655.
18. McCormick DA, Connors BW, Lighthill JW, Prince DA (1985) Comparative electrophysiology of pyramidal and sparsely spiny stellate neurons of the neocortex. *J Neurophysiol* 54:782–806.
19. Kawaguchi Y, Kubota Y (1993) Correlation of physiological subgroups of nonpyramidal cells with parvalbumin- and calbindin-D28k-immunoreactive neurons in layer V of rat frontal cortex. *J Neurophysiol* 70:387–396.
20. Porter JT, et al. (1998) Properties of bipolar VIPergic interneurons and their excitation by pyramidal neurons in the rat neocortex. *Eur J Neurosci* 10:3617–3628.
21. Xu HT, Pan F, Yang G, Gan WB (2007) Choice of cranial window type for *in vivo* imaging affects dendritic spine turnover in the cortex. *Nat Neurosci* 10:549–551.
22. Imai Y, Ibata I, Ito D, Ohsawa K, Kohsaka S (1996) A novel gene *iba1* in the major histocompatibility complex class III region encoding an EF hand protein expressed in a monocytic lineage. *Biochem Biophys Res Commun* 224:855–862.
23. Debus E, Weber K, Osborn M (1983) Monoclonal antibodies specific for glial fibrillary acidic (GFA) protein and for each of the neurofilament triplet polypeptides. *Differentiation* 25:193–203.
24. Grutzendler J, Kasthuri N, Gan WB (2002) Long-term dendritic spine stability in the adult cortex. *Nature* 420:812–816.
25. Holtmaat AJ, et al. (2005) Transient and persistent dendritic spines in the neocortex *in vivo*. *Neuron* 45:279–291.
26. Zuo Y, Lin A, Chang P, Gan WB (2005) Development of long-term dendritic spine stability in diverse regions of cerebral cortex. *Neuron* 46:181–189.
27. Majewska AK, Newton JR, Sur M (2006) Remodeling of synaptic structure in sensory cortical areas *in vivo*. *J Neurosci* 26:3021–3029.
28. Parra P, Gulyás AI, Miles R (1998) How many subtypes of inhibitory cells in the hippocampus? *Neuron* 20:983–993.
29. Dumitriu D, Cossart R, Huang J, Yuste R (2007) Correlation between axonal morphologies and synaptic input kinetics of interneurons from mouse visual cortex. *Cereb Cortex* 17:81–91.
30. Kawaguchi Y, Kubota Y (1997) GABAergic cell subtypes and their synaptic connections in rat frontal cortex. *Cereb Cortex* 7:476–486.
31. Amitai Y, et al. (2002) The spatial dimensions of electrically coupled networks of interneurons in the neocortex. *J Neurosci* 22:4142–4152.
32. Kawaguchi Y, Karube F, Kubota Y (2006) Dendritic branch typing and spine expression patterns in cortical nonpyramidal cells. *Cereb Cortex* 16:696–711.
33. Caulier LJ, Kulics AT (1991) The neural basis of the behaviorally relevant N1 component of the somatosensory-evoked potential in SI cortex of awake monkeys: Evidence that backward cortical projections signal conscious touch sensation. *Exp Brain Res* 84:607–619.
34. Caulier L (1995) Layer I of primary sensory neocortex: Where top-down converges upon bottom-up. *Behav Brain Res* 71:163–170.
35. Burkhalter A (1989) Intrinsic connections of rat primary visual cortex: Laminar organization of axonal projections. *J Comp Neurol* 279:171–186.
36. Herkenham M (1980) Laminar organization of thalamic projections to the rat neocortex. *Science* 207:532–535.
37. Antonini A, Fagiolini M, Stryker MP (1999) Anatomical correlates of functional plasticity in mouse visual cortex. *J Neurosci* 19:4388–4406.
38. Gilbert CD, Wiesel TN (1992) Receptive field dynamics in adult primary visual cortex. *Nature* 356:150–152.
39. Diamond ME, Huang W, Ebner FF (1994) Laminar comparison of somatosensory cortical plasticity. *Science* 265:1885–1888.
40. Das A, Gilbert CD (1995) Long-range horizontal connections and their role in cortical reorganization revealed by optical recording of cat primary visual cortex. *Nature* 375:780–784.
41. Rioult-Pedotti M, Friedman D, Hess G, Donoghue JP (1998) Strengthening of horizontal cortical connections following skill learning. *Nat Neurosci* 1:230–234.
42. De Paola V, et al. (2006) Cell type-specific structural plasticity of axonal branches and boutons in the adult neocortex. *Neuron* 49:861–875.
43. Stettler DD, Yamahachi H, Li W, Denk W, Gilbert CD (2006) Axons and synaptic boutons are highly dynamic in adult visual cortex. *Neuron* 49:877–887.
44. Ramachandran VS, Rogers-Ramachandran D, Stewart M (1992) Perceptual correlates of massive cortical reorganization. *Science* 258:1159–1160.
45. Jacobs KM, Donoghue JP (1991) Reshaping the cortical motor map by unmasking latent intracortical connections. *Science* 251:944–947.
46. Chklovskii DB, Mel BW, Svoboda K (2004) Cortical rewiring and information storage. *Nature* 431:782–788.
47. Wonders CP, Anderson SA (2006) The origin and specification of cortical interneurons. *Nat Rev Neurosci* 7:687–696.
48. Rutherford ES, Cline HT (2002) Multiphoton Imaging of Neurons in Living Tissue: Acquisition and Analysis of Time-Lapse Morphological Data. *Real-Time Imag* 8:175–188.
49. Tsiola A, Hamze-Sichani F, Peterlin Z, Yuste R (2003) Quantitative morphologic classification of layer V neurons from mouse primary visual cortex. *J Comp Neurol* 461:415–428.
50. Ward JH (1963) Hierarchical grouping to optimize an objective function. *J Am Stat Assoc* 58:236–244.